THE JOURNAL OF PHYSICAL CHEMISTRY B

Article

pubs.acs.org/JPCB

Theoretical Elucidation of the Origin for Assembly of the DAP12 Dimer with Only One NKG2C in the Lipid Membrane

Hui Sun, Huiying Chu, Ting Fu, Hujun Shen, and Guohui Li*

State key Laboratory of Molecular Reaction Dynamics, Dalian Institute of Chemical Physics, Chinese Academy of Sciences, 457 Zhongshan Rd., Dalian, 116023, P. R. China

Supporting Information

ABSTRACT: In this work, we have investigated in details the origin of the assembly of the DAP12 dimer with only one NKG2C in the activating immunoreceptor complex from thew two aspects of electronic properties and dynamic structures by performing density functional theory (DFT) calculations and molecular dynamics (MD) simulations. In the DFT calculations, we studied the aggregation ability of the $NKG2C_{TM}$ with the $DAP12_{TM}$ dimer and the $DAP12_{TM}$–$DAP12_{TM}$–$NKG2C_{TM}$ complex by analyzing the electrostatic potentials and frontier molecular orbitals (FMOs), and in the MD simulations we mainly investigated the dynamic structures of the $DAP12_{TM}$–$DAP12_{TM}$–$NKG2C_{TM}$ complex and its mutants, as well as the tetramer complex consisting of two $DAP12_{TM}$ and two $NKG2C_{TM}$ helixes without any restriction. Through the studies of the electrostatic potential, the FMOs, and the dynamic structures, we have provided reasonable explanations to some extent for the experimental observation that only one NKG2C can associate with the DAP12 homodimer. The present theoretical results are expected to give valuable information for further studying the assembly between receptors and signaling subunits.

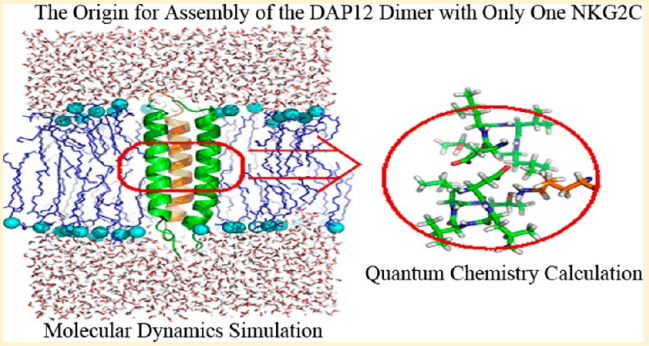

1. INTRODUCTION

It is well-known that the CD94/NKG2C heterodimer, consisting of a natural killer (NK) group 2C (NKG2C) and an invariant CD94 glycoprotein,[1] can function as an activating receptor[2,3] to assemble noncovalently with the DNAX activating protein 12 (DAP12), a disulfide-bonded homodimer, for cell surface expression and signaling.[4−6] This can be mainly attributed to the electrostatic interactions between one positively charged Lys residue in the transmembrane regions of NKG2C and two Asp residues of the immunoreceptor tyrosine-based activation motif (ITAM)[7] of adaptor molecule DAP12.[8−10]

Recently, Call et al.[11] has characterized the nuclear magnetic resonance (NMR) structure of the membrane-embedded heterotrimeric complex $DAP12_{TM}$–$DAP12_{TM}$–$NKG2C_{TM}$. In their work, mutagenesis studies uncovered that the assembly of the $DAP12_{TM}$–$DAP12_{TM}$–$NKG2C_{TM}$ complex was contributed by a more complex electrostatic network that existed among five hydrophilic residues, involving two Asp and two Thr residues in $DAP12_{TM}$ homodimer and one Lys residue in $NKG2C_{TM}$, instead of the simple salt bridge formed between the Lys residue of $NKG2C_{TM}$ and Asp residues of $DAP12_{TM}$. The study by Call et al.[11] provided a exquisite insight into how $NKG2C_{TM}$ assembles with $DAP12_{TM}$ homodimer. However, the question of why only one $NKG2C_{TM}$ can associate with the $DAP12_{TM}$ homodimer is still unclear from the obtained NMR structure. The major reason was speculated to may be an asymmetric redistribution of electronegativity on the two faces of the $DAP12_{TM}$ homodimer, which is caused by the assembly of the first $NKG2C_{TM}$ with the $DAP12_{TM}$ homodimer.

More recently, Cheng et al.[12] has performed nuclear Overhauser effect (NOE) based restrained molecular dynamics (MD) simulations to refine the $DAP12_{TM}$–$DAP12_{TM}$–$NKG2C_{TM}$ structure obtained by Call et al.[11] in both explicit micelles and bilayers. It is found that great changes have taken place in the side-chain conformation of $DAP12_{TM}$ homodimer during the simulation. Unlike the NMR structure of the $DAP12_{TM}$–$DAP12_{TM}$–$NKG2C_{TM}$ complex, both Asp residues in the $DAP12_{TM}$ homodimer can form stable salt bridges with the Lys residue of only $NKG2C_{TM}$ in the MD refined structures, and thus, there are no more Asp residues in the $DAP12_{TM}$ homodimer to interact with the second NKG2C, which may be a plausible explanation for the fact that only one NKG2C pairs with the DAP12 homodimer.

In order to clearly understand the origin for assembly of the DAP12 dimer with only one NKG2C in the activating immunoreceptor complex, we have investigated the electronic and dynamic structures of the $DAP12_{TM}$–$DAP12_{TM}$–$NKG2C_{TM}$ complex in detail by mean of density functional theory (DFT) calculations and classical molecular dynamic

Received: December 16, 2012
Revised: April 3, 2013
Published: April 5, 2013

dx.doi.org/10.1021/jp312375g | J. Phys. Chem. B 2013, 117, 4789−4797

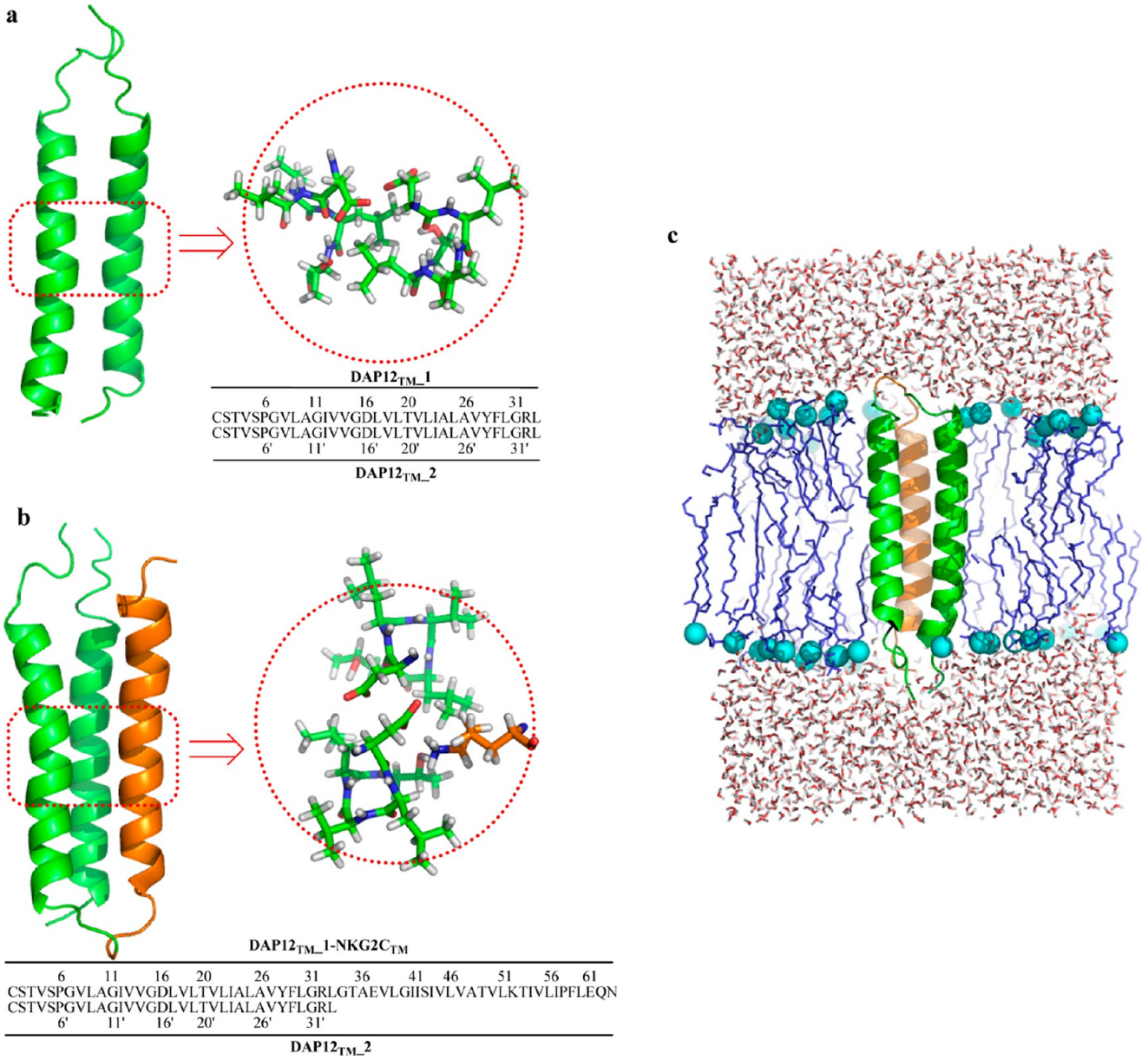

Figure 1. (a, b) The computational modes of the $DAP12_{TM}$-$DAP12_{TM}$ dimer and the $DAP12_{TM}$–$DAP12_{TM}$–$NKG2C_{TM}$ complex for DFT calculations. (c) Side view of the model systems for molecular dynamic simulations.

(MD) simulations, respectively. The theoretical results given in this work are expected to provide a reasonable explanation for the above experimental observation and to give valuable information for further studying the assembly between receptors and signaling subunits.

2. COMPUTATIONAL MODELS AND METHODS

The starting structures of the $DAP12_{TM}$ homodimer and the $DAP12_{TM}$–$DAP12_{TM}$–$NKG2C_{TM}$ complex were obtained from the average NMR structures (PDB codes 2L34 and 2L35),[11] where hydrogens were removed and added again in the program AMBER10.[13] The treated structures were assessed by the program H++[14] to predict the protonation states of the amino acid residues at pH 7.0, which agrees with the NMR experiments.[11] In the treated structures, the key Asp16/16′ residues are deprotonated, and the Lys52 is protonated. For the sake of convenience, the $DAP12_{TM}$ connecting with $NKG2C_{TM}$ is indicated as $DAP12_{TM}$_1 (the residues 1–33 in Figure 1), and another one is marked as $DAP12_{TM}$_2 (the residues 1′-33′ in Figure 1). Mutations with substitution of alanine for aspartic acid at positions 16/16′ (D16A) and for threonine at position 20/20′ (T20A) were modified using the Sybyl x1.1 software.

2.1. Quantum Chemistry Calculations. In order to obtain the electronic structure to explain the above experimental observation, we performed DFT calculations, before which an energy minimization was first carried out to remove close contacts in the starting geometries with constraining backbone atoms. Considering the complexity of models and computational cost in DFT calculation, the optimized structures of the $DAP12_{TM}$ homodimer and the $DAP12_{TM}$–$DAP12_{TM}$–$NKG2C_{TM}$ complex obtained from the energy minimization were truncated by removing components except for the residues 16–20 and 16′–20′ of two $DAP12_{TM}$ strands and Lys52 of $NKG2C_{TM}$ strand in active site. The corresponding computational models are shown in Figure 1a,b. Then, natural bond orbital (NBO) analysis[15,16] was performed

dx.doi.org/10.1021/jp312375g | J. Phys. Chem. B 2013, 117, 4789–4797

to analyze the electronic properties of the truncated structures by using the B3LYP functional with the 6-31g(d,p) basis set. DFT calculations were completed using the Gaussian 09 program package.[17]

2.2. Molecular Dynamics Simulation. The proteins (the starting structures of the $DAP12_{TM}$–$DAP12_{TM}$–$NKG2C_{TM}$ complex and its mutations) were first fitted into the DPPC lipid bilayer to generate the suitable membrane systems. Then the protein/DPPC systems were immerged in a cubic periodic solvent box filled with SPC water molecules.[18] A minimal distance of 12 Å between the surface of each simulated structure and the edge of solvent box was employed. Finally, Na^+ or Cl^- ions were added to maintain the charge neutrality of the modeled systems. The side view of the simulated system is shown in Figure 1c.

All MD simulations were carried out by using the Gromacs-4.0.5 package.[19,20] The united-atom GROMOS96 53a6 force field[21] was applied to the protein, and the united-atom force field for the lipid was adopted from previous MD studies of lipid bilayers.[22] The energy minimization with constraining no-solvent atoms was followed by the minimization of the whole system for a few thousand steps to remove conflicting contacts. Subsequently, the equilibrations of the systems were performed with gradually releasing the position restraints on the protein + lipid (1 ns), protein (10 ns), main chain (1 ns), and Cα (1 ns) of protein. Finally, for each system, five independent MD simulations were carried out for 40 ns, so the total simulation time for each system reached to 200 ns. All the simulations were performed under *NPT* conditions. The linear constraint solver (LINCS) method[23] was used to constrain the bonds associating with H atoms, and the integration time step was set to 2 fs. Electrostatic interactions were calculated using the particle–mesh Ewald (PME) algorithm.[24,25] To maintain a constant temperature of 300 K, the Nose–Hoover thermostat[26] was applied with a coupling time of 0.1 ps. Furthermore, the Parrinello–Rahman barostat[27] was employed with semi-isotropic scaling. A constant pressure of 1 bar was adopted in *X*/*Y* and *Z* directions, respectively.

3. RESULTS AND DISCUSSIONS

3.1. Quantum Chemistry Calculations. According to the proposals of Call et al.,[11] we have investigated in detail the electronic properties of the computation models for the $DAP12_{TM}$–$DAP12_{TM}$ dimer, the $DAP12_{TM}$–$DAP12_{TM}$–$NKG2C_{TM}$ complex, and the $NKG2C_{TM}$ by performing DFT calculations. The computational results are expected to some extent to provide a reasonable explanation for the assembly of the DAP12 homodimer with only one NKG2C.

The electrostatic potentials of the $DAP12_{TM}$–$DAP12_{TM}$ dimer, the $DAP12_{TM}$–$DAP12_{TM}$–$NKG2C_{TM}$ complex, and the $NKG2C_{TM}$ are given in Figure 2. As shown in the figure, two Asp16/16′ residues in the wild-type $DAP12_{TM}$ dimer carry almost equal, more negative charges, while the Lys52 residue in $NKG2C_{TM}$ has more positive charge. It is obvious that both Asp16/16′ residues in the wild-type $DAP12_{TM}$ dimer are able to attract the positively charged Lys residue in the transmembrane regions of NKG2C. When one $NKG2C_{TM}$ pairs with the $DAP12_{TM}$ dimer, it is found that the negative charges on two Asp16/16′ residues in the $DAP12_{TM}$–$DAP12_{TM}$–$NKG2C_{TM}$ complex significantly reduce. Therefore, the ability of two Asp16/16′ residues to attract the second positively charged Lys residue visibly diminishes, which is a reasonable explanation for the question why only one NKG2C can associate with the DAP12 homodimer.

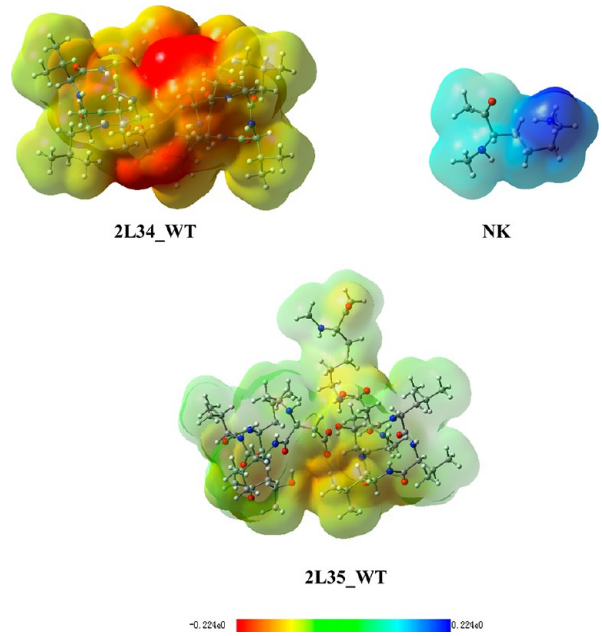

Figure 2. The electrostatic potentials of the models for 2L34_WT, 2L35_WT, and NK mapped on the molecular isodensity surface (ρ = 0.02 au): 2L34_WT, the wild-type $DAP12_{TM}$–$DAP12_{TM}$ complex; 2L35_WT, the wild-type $DAP12_{TM}$–$DAP12_{TM}$–$NKG2C_{TM}$ complex; NK, the wild-type $NKG2C_{TM}$. Color scheme ranges from red (−0.224 au) via green to blue (0.224 au).

Furthermore, we have also analyzed the frontier molecular orbitals (FMO) for the $DAP12_{TM}$–$DAP12_{TM}$ dimer, the $DAP12_{TM}$–$DAP12_{TM}$–$NKG2C_{TM}$ complex, and the $NKG2C_{TM}$. It is generally known that the interaction between two molecules can be understood through the FMO theory.[28,29] The strength of interaction between two molecules is inversely proportional to the energy difference between the highest occupied molecular orbitals (HOMOs) [the lowest unoccupied molecular orbitals (LUMOs)] of one molecule and the LUMOs (HOMOs) of the other. The smaller the HOMO–LUMO difference is, the stronger the interaction between two molecules is. As shown in Figure 3, the interaction between Lys52 residue of $NKG2C_{TM}$ and Asp16/16′ residues of $DAP12_{TM}$ dimer mainly occurs between the LUMO+1 of $NKG2C_{TM}$ and the HOMO of $DAP12_{TM}$ dimer, which can be understood from two aspects. On one hand, the LUMO+1 of $NKG2C_{TM}$ is an antibonding σ_{N-C} orbital on the side chain of the positively charged Lys residue, while the HOMO of $DAP12_{TM}$ dimer is a p orbital on O atom of one Asp residue. The LUMO+1 of $NKG2C_{TM}$ is able to effectively interact with the HOMO of $DAP12_{TM}$ dimer through head-to-head overlap from one side of the $DAP12_{TM}$ dimer, and thus, the partial charge on the negatively charged Asp residue can transfer from the HOMO of $DAP12_{TM}$ dimer to the LUMO+1 of $NKG2C_{TM}$. On the other hand, the energy difference of the two orbitals is the least, indicating that the interaction between the two orbitals is strongest. The FMO orbitals of the $DAP12_{TM}$–$DAP12_{TM}$–$NKG2C_{TM}$ complex and the $NKG2C_{TM}$ are given in Figure 4. Similar to the above results, the interaction between the Lys residue of $NKG2C_{TM}$ and the Asp residue of $DAP12_{TM}$–$DAP12_{TM}$–$NKG2C_{TM}$ complex also occurs between the LUMO+1 of $NKG2C_{TM}$ and the HOMO

dx.doi.org/10.1021/jp312375g | J. Phys. Chem. B 2013, 117, 4789–4797

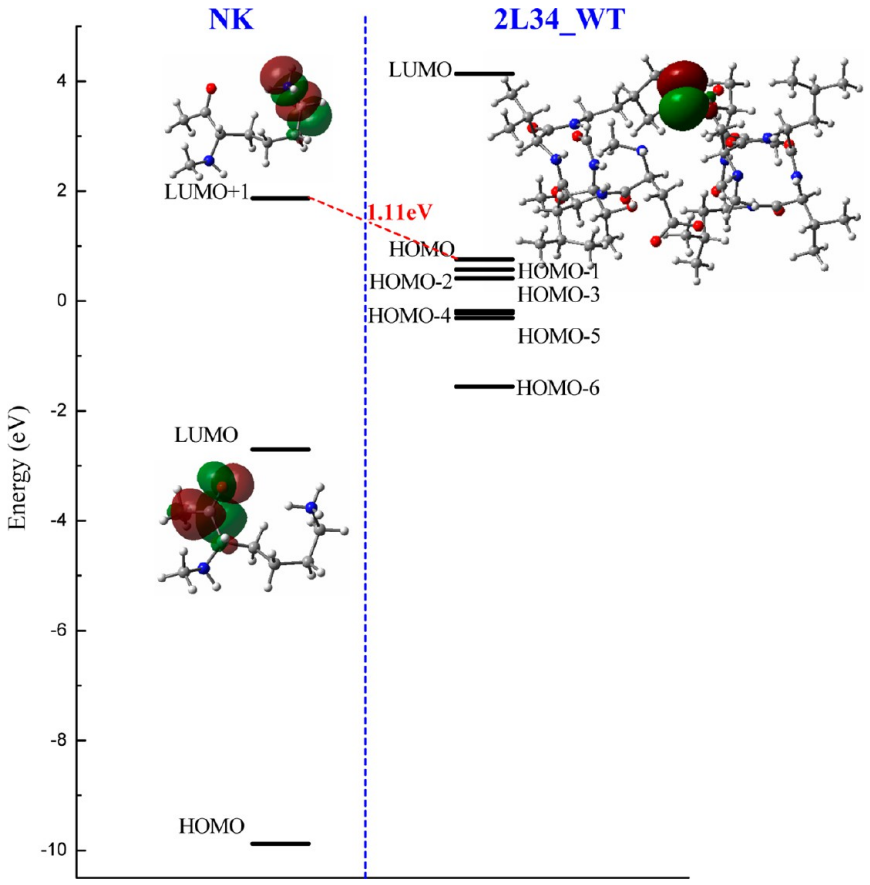

Figure 3. The frontier molecular orbitals for the models of NK and 2L34_WT. Isosurfaces are at 0.02.

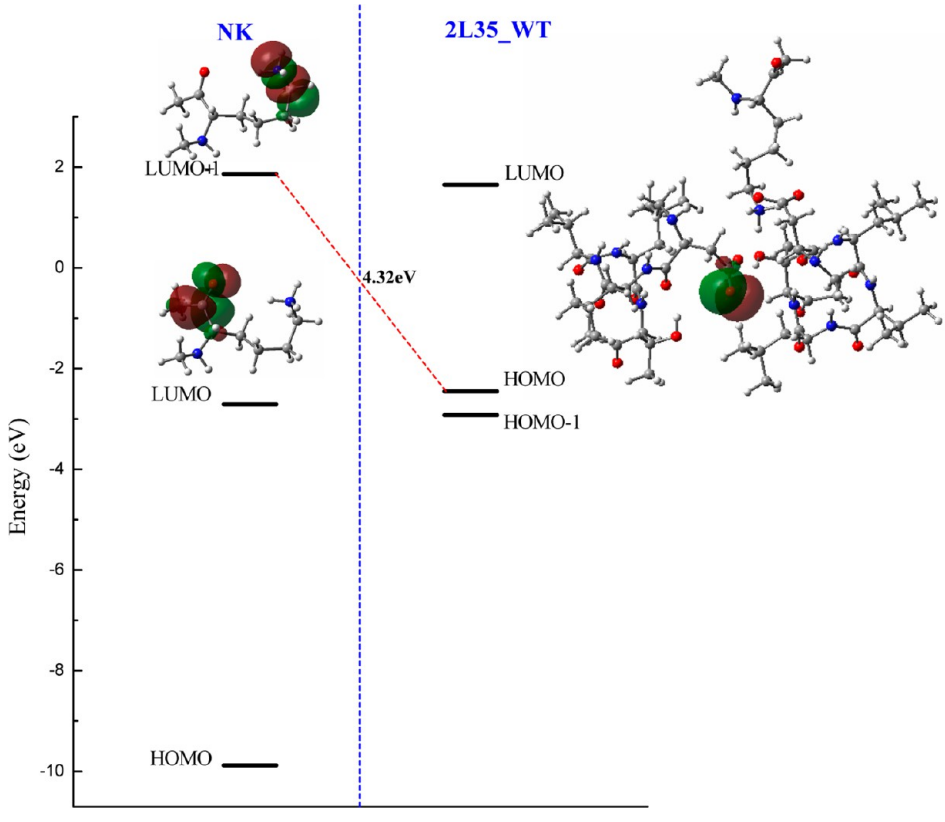

Figure 4. The frontier molecular orbitals for the models of NK and 2L35_WT. Isosurfaces are at 0.02.

dx.doi.org/10.1021/jp312375g | J. Phys. Chem. B 2013, 117, 4789−4797

of the $DAP12_{TM}$–$DAP12_{TM}$–$NKG2C_{TM}$ complex. However, the energy difference of the two orbitals is 4.32 eV, larger by 3.21 eV than that between the LUMO+1 of $NKG2C_{TM}$ and the HOMO of $DAP12_{TM}$ dimer, implying that the second $NKG2C_{TM}$ is difficult to assemble with the $DAP12_{TM}$–$DAP12_{TM}$–$NKG2C_{TM}$ complex. The theoretical results provide a reasonable explanation for the assembly of the DAP12 homodimer with only one NKG2C again.

3.2. Molecular Dynamic Simulation. Although we have given reasonable explanations for assembly of the DAP12 dimer with only one NKG2C from the electronic structures, the role of Thr20/20′ residues in the assembly process is still unclear, which was indicated to also have an important influence on the assembly of the DAP12 dimer with one NKG2C by Call et al.[11] In this section, we explored the dynamic structures of the $DAP12_{TM}$–$DAP12_{TM}$–$NKG2C_{TM}$ complex and its mutants without any restriction to investigate the origin in more detail for assembly of the DAP12 dimer with only one NKG2C.

As a measure of structural stability, the root-mean-square deviations (RMSD) from the starting structure were calculated for all backbone heavy atoms of the $DAP12_{TM}$–$DAP12_{TM}$–$NKG2C_{TM}$ complex and its mutants with substitution of alanine for aspartic acid at positions 16/16′ and for threonine at position 20/20′ against simulation time, and the RMSD curves are plotted in Figure 5. Through observation, it is found that plateaus in all simulated systems are almost reached after an initial increase during an equilibration period for the first 30 ns, indicating that stable and equilibrated protein structures are obtained. Therefore, the last 10 ns trajectories were used in the subsequent dynamic analyses.

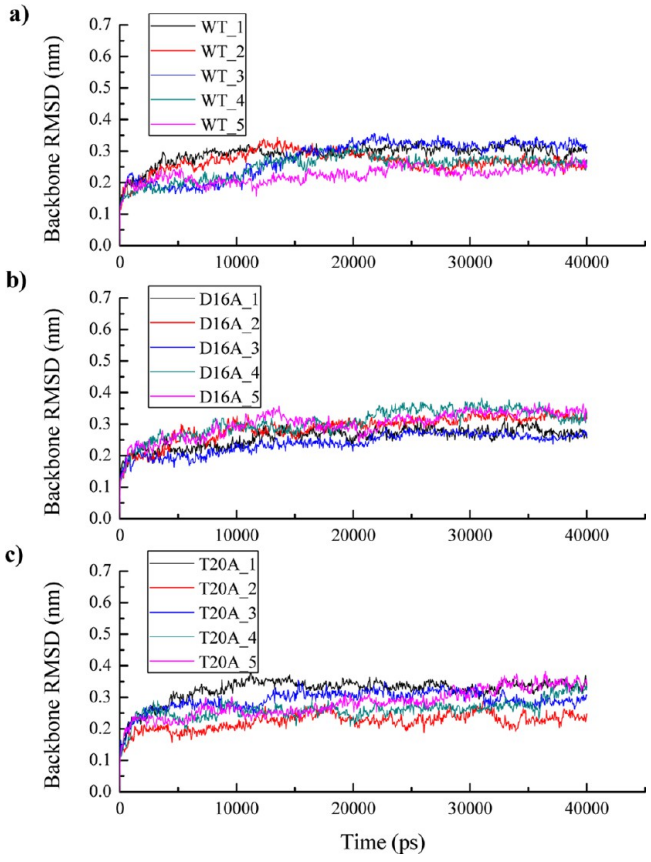

Figure 5. Time dependence of backbone RMSD for (a) the wild-type $DAP12_{TM}$–$DAP12_{TM}$–$NKG2C_{TM}$ complex, (b) the $DAP12_{TM}$–$DAP12_{TM}$–$NKG2C_{TM}$ complex with substitution of alanine for aspartic acid at positions 16 and 16′, and (c) the $DAP12_{TM}$–$DAP12_{TM}$–$NKG2C_{TM}$ complex with substitution of alanine for threonine at positions 20 and 20′.

Clustering analysis, in which the RMSD-based GROMOS algorithm[30] was used, was first performed to study the conformations of the $DAP12_{TM}$–$DAP12_{TM}$–$NKG2C_{TM}$ complex. A cutoff of 0.078 nm was selected for the analysis of the MD trajectories. Each structure in the trajectories will be classified to a cluster when its distance to any element is less than the given cutoff, and each cluster has a representative structure. We analyzed all five trajectories, and the conclusions obtained from the clustering analysis on the five trajectories are in perfect accord. Thus, we only take one trajectory to make a detailed introduction. Other results are shown in Figures S1 and S2 (Supporting Information).

Clustering analysis on the trajectory results in a total of 10 clusters. The representative structure of the largest cluster is shown in Figure 6a, which represents 39.2% of the snapshots from the trajectory. Compared with the average NMR structure of the $DAP12_{TM}$–$DAP12_{TM}$–$NKG2C_{TM}$ complex (**2L35**$_T$ and **2L35**$_S$), the side-chain conformations of Asp16/16′, Thr20/20′, and Lys52 residues have undergone dramatic changes, as shown in Figure 6b. In the representative structure, two Asp residues in the $DAP12_{TM}$ homodimer keep away from each other owing to the electrostatic repulsion (Figure 6a,b); however, both of them orient toward Lys52 due to the electrostatic attraction between Asp and Lys residues. As shown by $\mathbf{A}_T$ and $\mathbf{A}_S$ in Figure 6a, the side chain of the Lys52 residue is located between the side chains of two Asp residues, and the side chains of Asp16/16′ lie above and below the side chain of the Lys52 residue, respectively. This structure is helpful to diminish the repulsive energy between Asp16/16′ residues and increase the interaction energy between Asp16/16′ and Lys52. Ultimately, stable salt bridges between the side chains of Asp16/16′ and Lys52 residues are observed and confirmed by the distance evolutions of the side chain N atom of Lys52 with the side chain carboxyl C atoms of Asp16/16′ along simulation time in Figure 6b and the hydrogen bond occupancy between Asp16/16′ and Lys52 residues in Table 1. Therefore, we can conclude from the classic MD simulation that both Asp16/16′ residues in the $DAP12_{TM}$ homodimer can form stable salt bridges with the Lys52 residue of the first $NKG2C_{TM}$, and thus there are no more Asp residues in the $DAP12_{TM}$ homodimer to interact with the second $NKG2C_{TM}$, which is in good agreement with the finding of Cheng et al.[3]

Through further examination on the representative structure ($\mathbf{A}_T$ and $\mathbf{A}_S$), it is also found that the changes for the side chain conformations of Asp16/16′ and Lys52 residues led to the hydrogen bond interactions between Asp16′ and Thr20 residues, which can be proved by the hydrogen bond occupancy in Table 1. The hydrogen bond occupancy, calculated by the VMD software package, indicates the persistence of a specific hydrogen bond, i.e., the average fraction of time that hydrogen bonds are formed during the trajectory. From Table 1, it is very clear that the hydrogen bond occupancy between the side chains of Asp16′ and Thr20 residues is up to 104.12%, which implies that there are two possible hydrogen bonds between the side chains of Asp16′ and Thr20 residues. This fact indicates the existence of the highly stable hydrogen bonds between Asp16′ and Thr20 residues. In addition, the side chain O atom of Thr20 also interacts with the H atom on the side chain N atom of Lys52 to form a hydrogen bond, which has a hydrogen

dx.doi.org/10.1021/jp312375g | J. Phys. Chem. B 2013, 117, 4789–4797

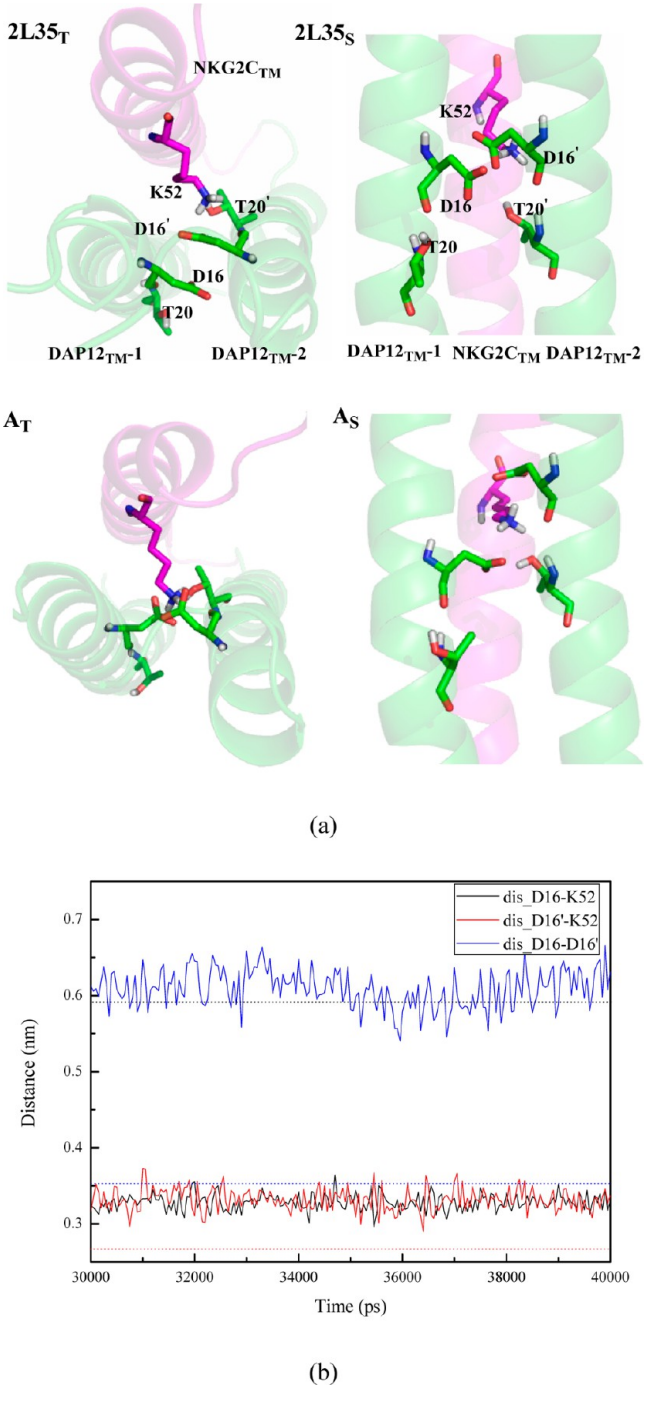

Figure 6. (a) The interaction between the key residues in the $DAP12_{TM}$–$DAP12_{TM}$–$NKG2C_{TM}$ complex before (**2L35**$_T$ and **2L35**$_S$) and after ($\mathbf{A}_T$ and $\mathbf{A}_S$) MD simulation. Subscripts T and S represent the top and side views of the $DAP12_{TM}$–$DAP12_{TM}$–$NKG2C_{TM}$ complex. (b) Distance between the key residues versus time. The dot and solid lines represent the distance between the key residues before (**2L35**$_T$ and **2L35**$_S$) and after ($\mathbf{A}_T$ and $\mathbf{A}_S$) MD simulation, respectively.

bond occupancy of 29.79%. Together, the Thr20 residue is considered to stabilize Asp16′ and Lys52 residues through the hydrogen bond interactions and thus contribute to the assembly of the DAP12 dimer with only one NKG2C. The results for the hydrogen bond analysis are also in good agreement with the finding of Cheng et al.[3] Furthermore, it is found that from Table 1 that there are hydrogen bonds

Table 1. Hydrogen Bond Occupancy between the Key Interfacial Residues[a] in the Wild-Type $DAP12_{TM}$–$DAP12_{TM}$–$NKG2C_{TM}$ Complex

donor	acceptor	occupancy (%)
K52-side	D16′-side	30.04
K52-side	D16-side	42.04
K52-side	D16-main	35.03
K52-side	T20-side	29.79
D16′-side	T20-side	104.12
D16′-side	T20-main	28.78
D16′-main	T20′-side	7.50
D16′-main	T20′-main	54.66
D16-main	T20-main	1.43

[a]"-side" and "-main" represent amino acid side chain and main chain, respectively.

between main chains of the key interfacial residues in the complex. Such interactions do not disturb the helical structures of the chains, which can be evaluated by calculating the secondary structure content of the $DAP12_{TM}$–$DAP12_{TM}$–$NKG2C_{TM}$ complex using the do_dssp tool in GROMACS (see Figure S3, Supporting Information), and are expected to contribute to the stability of the $DAP12_{TM}$–$DAP12_{TM}$–$NKG2C_{TM}$ complex.

Finally, we computed the interaction energies between $DAP12_{TM}$ dimer and $NKG2C_{TM}$ in the wild-type $DAP12_{TM}$–$DAP12_{TM}$–$NKG2C_{TM}$ complex (WT) and its mutants (D16A and T20A). The results are shown in Figure 7, where

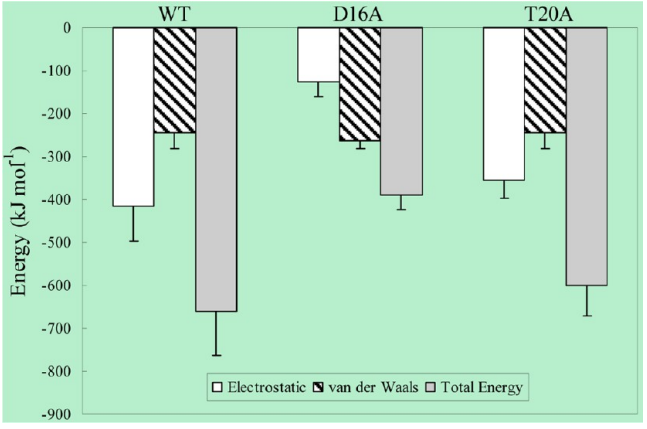

Figure 7. Interaction energy between the $DAP12_{TM}$ dimer and the $NKG2C_{TM}$. Error bars represent the standard deviation.

electrostatic interaction energies, van der Waals interaction energies, and total energies are listed, respectively. By comparing the interaction energies in the wild-type $DAP12_{TM}$–$DAP12_{TM}$–$NKG2C_{TM}$ complex and its mutants, it is found that the van der Waals interaction energies have scarcely changed in the three complexes, and major alterations take place in the electrostatic interaction energies, which eventually results in the change of total energies. The electrostatic interaction energies are arranged in descending order: WT > T20A > D16A. In the mutant D16A, two Asp16/16′ residues were replaced by alanine, which raises the loss of the electrostatic interaction between Asp16/16′ residues of $DAP12_{TM}$ dimer and the Lys52 residue of $NKG2C_{TM}$ and thus results in the sharp decrease of electrostatic interaction energy between $DAP12_{TM}$ dimer and $NKG2C_{TM}$. Therefore, Asp16/

dx.doi.org/10.1021/jp312375g | J. Phys. Chem. B 2013, 117, 4789–4797

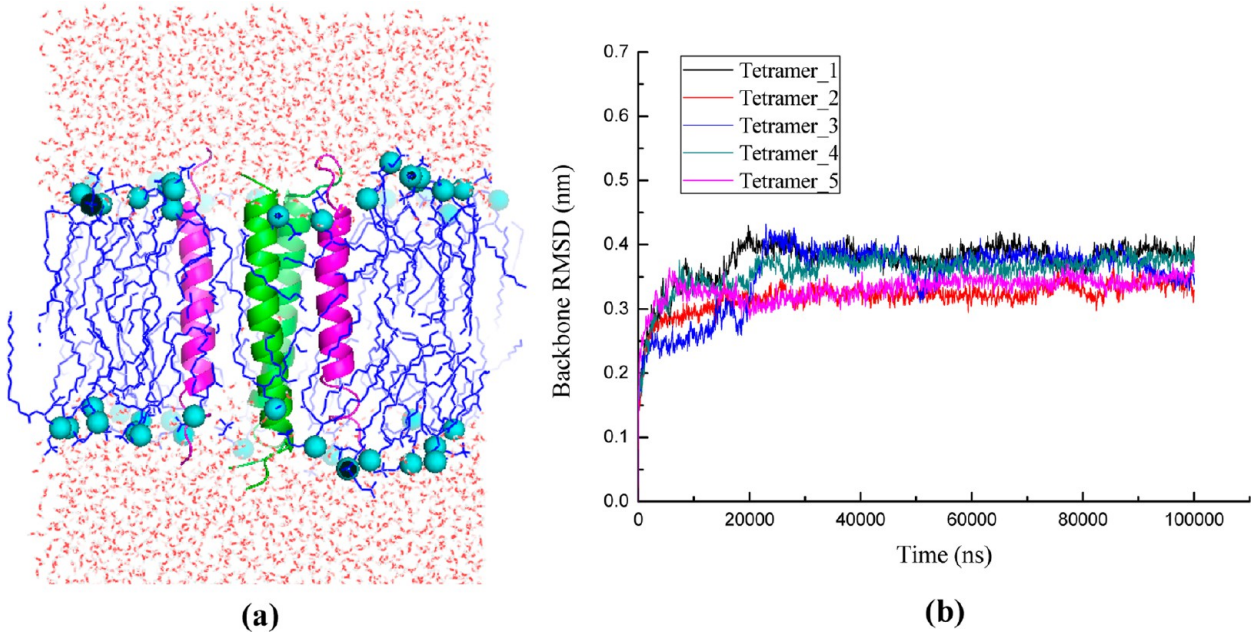

Figure 8. (a) Side view of the model systems for MD simulations on the system consisting of two $DAP12_{TM}$ and two $NKG2C_{TM}$ helixes. (b) Time dependence of backbone RMSD for the tetramer complex consisting of two $DAP12_{TM}$ and two $NKG2C_{TM}$ helixes.

16′ residues are considered to play the most important roles in the assembly process of DAP12 dimer with one NKG2C. Furthermore, the substitution of alanine for threonine at position 20/20′ also makes the electrostatic interaction energy between $DAP12_{TM}$ dimer and $NKG2C_{TM}$ lessen. Thus, it is expected that Thr20/20′ residues assist Asp16/16′ residues to complete the assembly of DAP12 dimer with one NKG2C.

To sum up, both Asp16/16′ residues in the $DAP12_{TM}$ homodimer are found to form stable salt bridges with the Lys52 residue of the first $NKG2C_{TM}$, and thus there are no more Asp residues in the $DAP12_{TM}$ homodimer to interact with the second $NKG2C_{TM}$, which is the major cause for assembly of the DAP12 dimer with only one NKG2C. In addition, Thr20/20′ residues stabilize Asp16′ and Lys52 residues through the hydrogen bond interactions and make the minor contribution to the assembly of the DAP12 dimer with only one NKG2C.

In addition, to further investigate the possibility/impossibility that two DAP12 and two NKG2C form a stable complex, five independent MD simulations on the system consisting of two $DAP12_{TM}$ and two $NKG2C_{TM}$ helixes have been performed for 100 ns, respectively. The side view of the simulated system, where the location of the second $NKG2C_{TM}$ relative to the $DAP12_{TM}$ dimer is similar to that of the first $NKG2C_{TM}$, is shown in Figure 8a. The computational methods are in accord with those used in MD simulations on the systems of the $DAP12_{TM}$–$DAP12_{TM}$–$NKG2C_{TM}$ complex. The RMSD from the starting structure are calculated, which are plotted in Figure 8b. Through observation, it is found that equilibrations in all simulated systems are almost reached after 30 ns. During the simulations, the expected unstable tetramer complex consisting of two $DAP12_{TM}$ and two $NKG2C_{TM}$ helixes can not be observed on the simulation time scale. This also can be obtained from the distance analysis between the key residues (Figure S4, Supporting Information) and the secondary structure analysis for the tetramer complex consisting of two $DAP12_{TM}$ and two $NKG2C_{TM}$ helixes (Figure S5, Supporting Information). Finally, we compared the interaction energies between $DAP12_{TM}$ dimer and $NKG2C_{TM}$ in the wild-type $DAP12_{TM}$–$DAP12_{TM}$–$NKG2C_{TM}$ complex and the tetramer complex consisting of two $DAP12_{TM}$ and two $NKG2C_{TM}$ helixes (as shown in Table S1, Supporting Information). The interaction energies (656.20 and 593.23 kJ mol^{-1}) between $DAP12_{TM}$ dimer and $NKG2C_{TM}$ in the tetramer complex are reduced a little, compared with that (697.24 kJ mol^{-1}) in the wild-type $DAP12_{TM}$–$DAP12_{TM}$–$NKG2C_{TM}$ complex. This is also not favorable evidence for the instability of the tetramer complex. Therefore, the MD simulations on the system consisting of two $DAP12_{TM}$ and two $NKG2C_{TM}$ helixes at the simulation time scale are not able to answer this critical question of why the DAP12 homodimer can associate with only one NKG2C. There are two possible reasons for this result. On one hand, a simulation time of 100 ns may be not long enough for the structural change of the tetramer complex. On the other hand, the GROMOS96 53a6 force field used in these simulations employs fixed partial charges, which cannot effectively describe the electrostatic interaction between $DAP12_{TM}$ dimer and $NKG2C_{TM}$ like DFT calculation. Thus, much longer simulation time or polarizable force fields may be needed to observe the instability of the tetramer complex consisting of two $DAP12_{TM}$ and two $NKG2C_{TM}$ helixes.

4. CONCLUSION

In this work, we have investigated in detail the origin for assembly of the DAP12 dimer with only one NKG2C in the activating immunoreceptor complex by performing DFT calculations and MD simulations.

In the DFT calcultions, we studied the aggregation ability of the $NKG2C_{TM}$ with the $DAP12_{TM}$ dimer and the $DAP12_{TM}$–$DAP12_{TM}$–$NKG2C_{TM}$ complex by analyzing the electrostatic potentials and the FMOs. From the distribution of the electrostatic potential, it is found that the negative charges on two Asp16/16′ residues in the $DAP12_{TM}$–$DAP12_{TM}$–$NKG2C_{TM}$ complex significantly reduce as compared with those in the $DAP12_{TM}$ dimer. Furthermore, according to the FMO analysis, the interactions of the $NKG2C_{TM}$ with the

dx.doi.org/10.1021/jp312375g | J. Phys. Chem. B 2013, 117, 4789–4797

$DAP12_{TM}$ dimer and the $DAP12_{TM}$–$DAP12_{TM}$–$NKG2C_{TM}$ complex will occur between the LUMO+1 of the $NKG2C_{TM}$ and the HOMO of the DAP12 dimer and the $DAP12_{TM}$–$DAP12_{TM}$–$NKG2C_{TM}$ complex, and the energy difference between the LUMO+1 of the $NKG2C_{TM}$ and the HOMO of the $DAP12_{TM}$–$DAP12_{TM}$–$NKG2C_{TM}$ complex is larger than that between the LUMO+1 of $NKG2C_{TM}$ and the HOMO of $DAP12_{TM}$ dimer. All the results obtained from DFT calculations indicated that the $DAP12_{TM}$ dimer can pair with only one $NKG2C_{TM}$.

Subsequently, in the MD simulations, we investigated the dynamic structures of the $DAP12_{TM}$–$DAP12_{TM}$–$NKG2C_{TM}$ complex and its mutants without any restriction. Both Asp16/16′ residues in the $DAP12_{TM}$ homodimer are found to form stable salt bridges with the Lys52 residue of the first $NKG2C_{TM}$, and thus, there are no more Asp residues in the $DAP12_{TM}$ homodimer to interact with the second $NKG2C_{TM}$, which is considered as the major cause for assembly of the DAP12 dimer with only one NKG2C. In addition, Thr20/20′ residues stabilize Asp16′ and Lys52 residues through the hydrogen bond interactions and make the minor contribution to the assembly of the DAP12 dimer with only one NKG2C. The MD simulations of 100 ns on the system consisting of two $DAP12_{TM}$ and two $NKG2C_{TM}$ helixes will be not able to answer this critical question as to why the DAP12 homodimer can associate with only one NKG2C. However, much longer simulation time or employing polarizable force fields is expected to be helpful to observe the instability of the tetramer complex consisting of two $DAP12_{TM}$ and two $NKG2C_{TM}$ helixes.

So far, the present theoretical results have provided reasonable explanations to some extent for the experimental observation that only one NKG2C can associate with the DAP12 homodimer in the lipid membrane and are expected to give valuable information for further studying the assembly between receptors and signaling subunits.

■ ASSOCIATED CONTENT

Supporting Information

The interaction between the key residues in the $DAP12_{TM}$–$DAP12_{TM}$–$NKG2C_{TM}$ complex, the evolution of distance between the key residues versus time, and a plot of secondary structure content as a function of time for the $DAP12_{TM}$–$DAP12_{TM}$–$NKG2C_{TM}$ complex and the tetramer complex consisting of two $DAP12_{TM}$ and two $NKG2C_{TM}$ helixes. This material is available free of charge via the Internet at http://pubs.acs.org.

■ AUTHOR INFORMATION

Corresponding Author

*E-mail: ghli@dicp.ac.cn.

Notes

The authors declare no competing financial interest.

■ ACKNOWLEDGMENTS

This work described in this paper is supported by the National Natural Science Foundations of China (Grants No. 31070641 and 21103168), 973 Program (2012CB721002) and 863 Program (2012AA01A305), "Hundreds Talents Program" of the Chinese Academy of Sciences.

■ REFERENCES

(1) Lazetic, S.; Chang, C.; Houchins, J. P.; Lanier, L. L.; Phillips, J. H. *J. Immunol.* **1996**, *157*, 4741–4745.
(2) Houchins, J. P.; Lanier, L. L.; Niemi, E.; Phillips, J. H.; Ryan, J. C. *J. Immunol.* **1997**, *158*, 3603–3609.
(3) Cantoni, C.; Biassoni, R.; Pende, D.; Sivori, S.; Accame, L.; Pareti, L.; Semenzato, G.; Moretta, L.; Moretta, A.; Bottino, C. *Eur. J. Immunol.* **1998**, *28*, 327–338.
(4) Campbell, K. S.; Cella, M.; Carretero, M.; Lopez-Botet, M.; Colonna, M. *Eur. J. Immunol.* **1998**, *28*, 599–609.
(5) Lanier, L. L.; Corliss, B. C.; Wu, J.; Leong, C.; Phillips, J. H. *Nature* **1998**, *391*, 703–707.
(6) Lanier, L. L.; Corliss, B.; Wu, J.; Phillips, J. H. *Immunity* **1998**, *8*, 693–701.
(7) Humphrey, M. B.; Lanier, L. L.; Nakamura, M. C. *Immunol. Rev.* **2005**, *208*, 50–65.
(8) Exley, M.; Terhorst, C.; Wileman, T. *Semin. Immunol.* **1991**, *3*, 283–297.
(9) Call, M. E.; Pyrdol, J.; Wiedmann, M.; Wucherpfenning, K. W. *Cell* **2002**, *111*, 967–979.
(10) Call, M. E.; Wucherpfenning, K. W. *Annu. Rev. Immunol.* **2005**, *23*, 101–125.
(11) Call, M. E.; Wucherpfenning, K. W.; Chou, J. J. *Nat. Immunol.* **2010**, *11*, 1023–1029.
(12) Cheng, X.; Lm, W. *Biophy. J.* **2012**, *102*, L27–L29.
(13) Case, D. A.; Darden, T. A.; Cheatham, T. E., III; Simmerling, C. L.; Wang, J.; Duke, R. E.; Luo, R.; Crowley, M.; Walker, R. C.; Zhang, W.; Merz, K. M.; Wang, B.; Hayik, S.; Roitberg, A.; Seabra, G.; Kolossváry, I.; Wong, K. F.; Paesani, F.; Vanicek, J.; Wu, X.; Brozell, S. R.; Steinbrecher, T.; Gohlke, H.; Yang, L.; Tan, C.; Mongan, J.; Hornak, V.; Cui, G.; Mathews, D. H.; Seetin, M. G.; Sagui, C.; Babin, V.; Kollman, P. A. *AMBER10*; University of California: San Francisco, 2008.
(14) Gordon, J. C.; Meyers, J. B.; Folta, T.; Shoja, V.; Heath, L. S.; Onufriev, A. *Nucleic Acids Res.* **2005**, *33*, W369–W371.
(15) Reed, A. E.; Weinstock, R. B.; Weinhold, F. *J. Chem. Phys.* **1985**, *83*, 735–746.
(16) Reed, A. E.; Curtiss, L. A.; Weinhold, F. *Chem. Rev.* **1988**, *88*, 899–926.
(17) Frisch, M. J.; Trucks, G. W.; Schlegel, H. B.; Scuseria, G. E.; Robb, M. A.; Cheeseman, J. R.; Scalmani, G.; Barone, V.; Mennucci, B.; Petersson, G. A.; Nakatsuji, H.; Caricato, M.; Li, X.; Hratchian, H. P.; Izmaylov, A. F.; Bloino, J.; Zheng, G.; Sonnenberg, J. L.; Hada, M.; Ehara, M.; Toyota, K.; Fukuda, R.; Hasegawa, J.; Ishida, M.; Nakajima, T.; Honda, Y.; Kitao, O.; Nakai, H.; Vreven, T.; Montgomery, J. A., Jr.; Peralta, J. E.; Ogliaro, F.; Bearpark, M.; Heyd, J. J.; Brothers, E.; Kudin, K. N.; Staroverov, V. N.; Kobayashi, R.; Normand, J.; Raghavachari, K.; Rendell, A.; Burant, J. C.; Iyengar, S. S.; Tomasi, J.; Cossi, M.; Rega, N.; Millam, J. M.; Klene, M.; Knox, J. E.; Cross, J. B.; Bakken, V.; Adamo, C.; Jaramillo, J.; Gomperts, R.; Stratmann, R. E.; Yazyev, O.; Austin, A. J.; Cammi, R.; Pomelli, C.; Ochterski, J. W.; Martin, R. L.; Morokuma, K.; Zakrzewski, V. G.; Voth, G. A.; Salvador, P.; Dannenberg, J. J.; Dapprich, S.; Daniels, A. D.; Farkas, O.; Foresman, J. B.; Ortiz, J. V.; Cioslowski, J.; Fox, D. J. *Gaussian 09*, Revision A.02; Gaussian, Inc.: Wallingford CT, 2009.
(18) Berendsen, H. J. C.; Postma, J. P. M.; van Gunsteren, W. F.; Hermans. J. *In Intermolecular Force*. Pullman, B., Ed.; Reidel: Dordrecht, The Netherlands, 1981; pp 331–342.
(19) Berendsen, H. J. C.; van der Spoel, D.; van Drunen, R. *Comput. Phys. Commun.* **1995**, *91*, 43–56.
(20) Van Der Spoel, D.; Lindahl, E.; Hess, B.; Groenhof, G.; Mark, A. E.; Berendsen, H. J. *J. Comput. Chem.* **2005**, *26*, 1701.
(21) Oostenbrink, C.; Villa, A.; Mark, A. E.; van Gunsteren, W. F. *J. Comput. Chem.* **2004**, *25*, 1656–1676.
(22) Berger, O.; Edholm, O.; Jähnig, F. *Biophys. J.* **1997**, *72*, 2002–2013.
(23) Hess, B.; Bekker, H.; Berendsen, H. J. C.; Fraaije, J. G. E. M. *J. Comput. Chem.* **1997**, *18*, 1463–1472.

(24) Darden, T.; York, D.; Pedersen, L. *J. Chem. Phys.* **1993**, *98*, 10089−10092.
(25) Essmann, U.; Perera, L.; Berkowitz, M. L.; Darden, T.; Lee, H.; et al. *J. Chem. Phys.* **1995**, *103*, 8577−8593.
(26) Hoover, W. *Phys. Rev. A* **1985**, *31*, 1695−1697.
(27) Parrinello, M.; Rahman, A. *J. Appl. Phys.* **1981**, *52*, 7182−7190.
(28) Fukui, K.; Fujimoto, H. *Frontier Orbitals and Reaction Path: Selected Papers of Kenichi Fukui*; World Scientific: Singapore, 1997.
(29) Hoffmann, R. *Rev. Mod. Phys.* **1988**, *60*, 601.
(30) Daura, X.; Gademann, K.; Jaun, B.; Seebach, D.; van Gunsteren, W.; Mark, A. *Angew. Chem. Int. Ed.* **1999**, *38*, 236−240.